Digital image correlation and topography data from analogue modelling experiments addressing the influence of basin geometry on gravity-driven salt tectonics at the Tectonic Modelling Lab of the University of Rennes (F) (https://doi.org/10.5880/fidgeo.2021.028)

Frank Zwaan[1,2,3]*, Matthias Rosenau[4], Daniele Maestrelli[5]

1. Géosciences Rennes, Unité Mixte de Recherche 6118, CNRS et Université de Rennes 1, Rennes, France
2. Dipartimento di Scienze della Terra, Università degli Studi di Firenze, Florence, Italy
3. Institute of Geological Sciences, University of Bern, Bern, Switzerland
4. Helmholtz Centre Potsdam - GFZ German Research Centre for Geosciences, Potsdam, Germany
5. Consiglio Nazionale delle Ricerche, Istituto di Geoscienze e Georisorse (CNR-IGG), Florence, Italy
* Corresponding author: frank.zwaan@geo.unibe.ch

1. Licence

2. Citation

When using the data please cite:

Zwaan, F., Rosenau, M., Maestrelli, D. (2021): Digital image correlation and topography data from analogue modelling experiments addressing the influence of basin geometry on gravity-driven salt tectonics at the Tectonic Modelling Lab of the University of Rennes (F). GFZ Data Services. https://doi.org/10.5880/fidgeo.2021.028

The data are supplementary material to:

Zwaan, F., Rosenau, M., Maestrelli, D. (2021). How initial basin geometry influences gravity-driven salt tectonics: Insights from laboratory experiments. Marine and Petroleum Geology, 105195. https://doi.org/10.1016/j.marpetgeo.2021.105195

Table of contents

3. Data Description

This data set includes the results of digital image correlation of 35 brittle-viscous experiments on gravitational salt tectonics performed at the Tectonic Modelling Lab of the University of Rennes 1 (UR1). The experiments demonstrate the influence of basin geometry on gravity-gliding style salt tectonics. Detailed descriptions of the experiments and basin geometries can be found in Zwaan et al. (submitted) to which this data set is supplementary. The models have been monitored by means of digital image correlation (DIC) analysis including Particle Image Velocimetry (PIV; Adam et al., 2005) and Structure-from-Motion photogrammetry (SfM; Donnadieu et al., 2003; Westoby et al., 2012). DIC analysis yields quantitative model surface deformation information by means of 3D surface topography and incremental and cumulative displacements. The data presented here consist of movies and images displaying the cumulative analogue model surface displacement, digital elevation models as well as profiles of the downslope incremental and cumulative displacements and surface elevation.

3.1. Monitoring and analysis methods

All experiments (Table 1) were monitored with top view photographs shot with 11 MPx SLR Cameras (Nikon D 80 and Canon Powershoot G11) every 15 (some 12) minutes during the 48-hour (or 49-hour) model runs. Additional perspective views were taken.

Table 1: Overview of experimental layout and parameters.

Experiment ID in Zwaan et al. (202x)	Mean layer thickness (mm³)	Run time (hh:mm)	Image interval (min)	Start time PIV* (min)	Cumulative PIV interval (images)	Incremental PIV interval (images)	DEM
Series I – 1° tilt – brittle cover layer							
A	5	48:00	15	00:00	4	32	x
B	5	48:00	15	00:00	4	32	x
C	5	48:00	15	00:00	4	32	x
D	5	48:00	15	00:15	4	32	x
E	5	48:00	15	00:15	4	32	x
F	8.3	48:00	15	01:30	4	32	x
G	7.5	48:00	15	01:30	4	32	x
H	6.7	48:00	15	01:30	4	32	x
I	3.8	48:00	15	00:00	4	32	x
J	3.3	48:00	15	00:00	4	32	x
Series II – 3° tilt – brittle cover layer							
K	5	48:00	15	00:15	4	32	x
L	5	48:00	15	00:15	4	32	x
M	5	48:00	15	00:15	4	32	x
N	5	48:00	15	00:00	4	32	x
O	5	48:00	15	00:00	4	32	x
P'	8.3	48:00	15	00:00	4	32	-
Q'	7.5	48:00	15	00:00	4	32	-
R'	6.7	48:00	15	00:00	4	32	-
S'	3.8	48:00	15	00:00	4	32	-
T'	3.3	48:00	15	00:15	4	32	-
U''	8.3	48:00	15	00:00	4	32	x
V''	7.5	48:00	15	00:00	4	32	x
W''	6.7	48:00	15	00:00	4	32	x
X''	3.8	48:00	15	00:00[#]	4	32	x
Y''	3.3	48:00	15	00:00[#]	4	32	x

Series III – 3° dip – no cover layer							
Z1	5	49:00	15	00:00	4	32	x
Z2	5	49:00	15	00:00	4	32	x
Z3	5	49:00	15	00:15	4	32	x
Z4	5	49:00	12	00:48	5	40	x
Z5	5	49:00	12	00:48	5	40	x
Z6	8.3	48:00	15	00:00	4	32	x
Z7	7.5	48:00	15	00:00	4	32	x
Z8	6.7	48:00	15	00:00	4	32	x
Z9	3.8	48:00	12	00:00	5	40	x
Z10	3.3	48:00	12	00:00	5	40	x

' and '' indicate repeating experiments, where no stereographic pictures of the former (and thus no DEMs) were available. *due to early camera shifts, some experiments could not be analyzed from the very beginning. The movies in this data set contain the initial increments. #shaking during the early phase

3.1.1. Particle Image Velocimetry (PIV)

Top view photographs of the experimental surface were analyzed with Particle Image Velocimetry (PIV; Adam et al., 2005) techniques to quantify horizontal displacements in the image plane at high precision and accuracy (< 0.1 mm). PIV was undertaken with the software DaVis 8.0 (LaVision) applying 2D-DIC least square methods algorithm (LSM) with subset and step sizes of 59 and 10 px, respectively. PIV intervals were chosen such that it corresponds to 1-hour and 8-hour intervals for cumulative (D_y) and incremental (V_y) displacements, respectively (Table 1). Cumulative displacements (D_y) have been calculated by means of adding the 1-hour increments in a Lagrangian reference frame (sum of differential). Note that some models miss the early stage in the PIV analysis because of rare shaking and camera shifts (Table 1). **NB:** the coordinate system used for the PIV results in this data publication differs from the coordinate system used by Zwaan et al. (2021); the PIV results in the Zwaan et al. (2021) publication are rotated 90° counterclockwise in map view with respect to the data presented here.

3.1.2. Structure from Motion (SfM)

Perspective photographs of our models were used to reconstruct the model 3D topography with the use of photogrammetry software (Agisoft Photoscan) (Figure 3). The method is based on Structure-from-Motion principle, commonly applied to analogue modelling (SfM, e.g., Donnadieu et al., 2003), which is able to align perspective photos of a subject and to reconstruct, via point cloud interpolation, its 3D surface and consequently the Digital Elevation Model (DEM) (Fig. 4). 3D models (i.e., model meshes) and DEMS of the initial and final model state were built according to the following workflow:

1) Minimum dataset of 11 photos uploaded for each model.
2) Automatic photo alignment: tie point cloud (sparse cloud) building.
3) Manual markers identification (4 markers) on a target photos.
4) Photo interpolation: dense cloud building (high resolution).
5) Point interpolation: mesh building (3D model).
6) Texture building on 3D model: 3D model pdf export (.pdf format).
7) Markers geo-reference procedure: local coordinates assignment and model rectification.
8) DEM building: from mesh surface to DEM (.tiff format)

Since the model surface was not always perfectly flat, normalized DEMs of the final model topography were produced by substracting the DEMs that represent the initial model state from the DEMs that represent the final state. Initial quality control was done by checking if the model boundaries in these normalized DEMs were at z = 0 level. If not, this was corrected by slightly tilting the normalized model. Subsequently the cut-and-fill volumes (volumes below and above the z = 0 level) were extracted and compared to ensure that both values were similar and if so, the normalized DEM was considered valid. Note that, in contrast to the PIV results, the DEMs use the same coordinate system as the Zwaan et al. (2021) publication.

3.2. Digital image correlation data

3.2.1. Surface displacement

Results of PIV analysis are 2D surface displacements accumulated over 1 h increments. These data are presented in the form of images of the final (after 48 h) cumulative surface displacement pattern (e.g. Figure 1) and movies showing the accumulation of surface displacement.
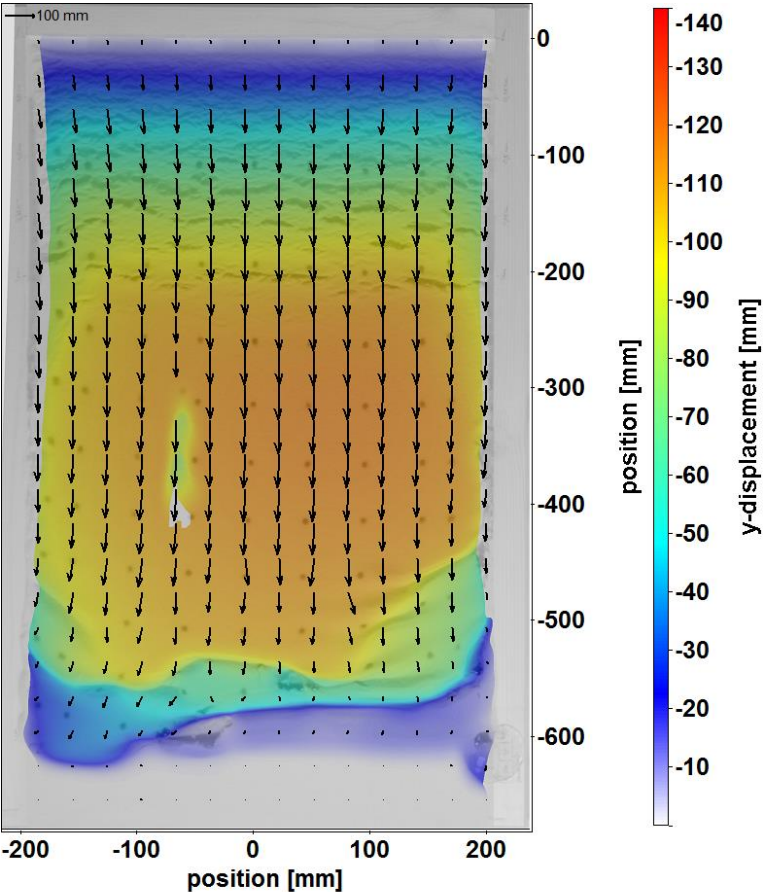
Figure 1: Example of final cumulative surface displacement from PIV (Model P). Color-coded map and vectors of cumulative down-slope (y-) displacement. Exaggeration of vectors according to reference vector top left. See movies included in this data set for evolution

The PIV-derived surface displacement field was further analyzed by extracting values of down-slope displacements along a central (x=0) profile parallel to the y-axis and picking its maximum. This procedure was done for both incremental displacements (Vy, MVP = maximum velocity point) and cumulative displacements (Dy, MDP = maximum displacement point) (Figure 2).
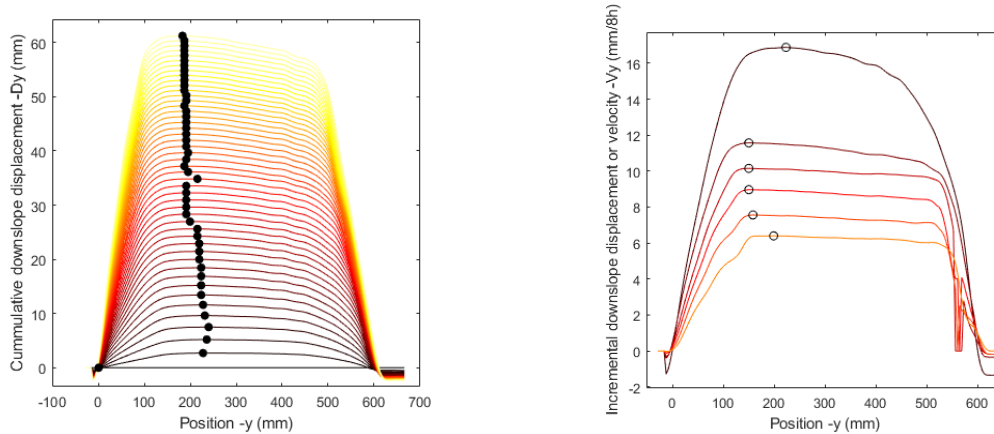
Figure 2: Example of cumulative (left) and incremental (right) displacement profile plot with MDP and MVP indicated (Model H). Temporal succession of the profiles indicated by colors (early = dark, late = bright).

Matlab-based scripts ("DyProfilesPlot.m" and "VyProfilesPlot.m") are provided to automatically visualize y-displacement Dy and velocity Vy along the profile and its maximum point location (MDP and MVP, respectively) for each time step in one diagram (Figure 2). The input files are named "ID_Vy-y-t_1h_x=0.prm" and "ID_Dy-y-t_1h_x=0.prm" for incremental and cumulative displacements, respectively.

Table 2: Example of Dy (cumulative data) and Vy (incremental data) profile data file. For each profile shown in the diagram, the profile position and values of the y-displacement are listed in two paired columns.

| position/mm	y-displacement/mm	position/mm	y-displacement/mm	…
30.855000	0.000000	30.855000	0.000000	…
27.137529	0.000000	27.137529	0.000000	…
…	…	…	…	…

3.2.2. Surface topography data (3D Meshes and DEMs)

The results of the SfM analysis are virtual reconstructions of the surface of the analogue experiments at the start and the end of a model run. The obtained dense point clouds were interpolated to create model mesh surfaces (Fig. 3), provided as a fully navigable 3D PDF files (.pdf) that can be used to visualize the three-dimensional architecture of each model. From the same dense cloud used for mesh reconstruction, DEMs showing the pre-deformation and final deformed surfaces of each model were calculated (Fig. 4). Subtracting the pre-deformation surface from the final deformed surface revealed the vertical change in topography throughout the model (normalized), provided as geotiff files (.tiff). These files represent the actual data used for normalized topographic profile extraction and analysis. An example of parameters used for the mesh interpolation and the DEM reconstruction are shown in Table 3. From left to right, the table reports the number of photos used for 3D model

5

reconstruction, the number of tie points generated by the photo alignment procedure (constituting the sparse cloud) and the number of points interpolated to build the dense cloud. The number of faces constituting the model mesh interpolated from the dense cloud is also shown. The table subsequently indicates the number of markers used for model georeferencing procedure (and respective local coordinates). The last two columns report the DEM resolution and the values obtained for the maximum reprojection error, this latter representing an estimate of the quality of three-dimensional points projection (the lower the value, the higher the quality of the sparse cloud).


Figure 3: Example of model 3D rendering obtained after SfM mesh interpolation (Model H, t=48h). *Note that these files are for 3D visualization, but do not allow for analysis (see Fig. 4).*
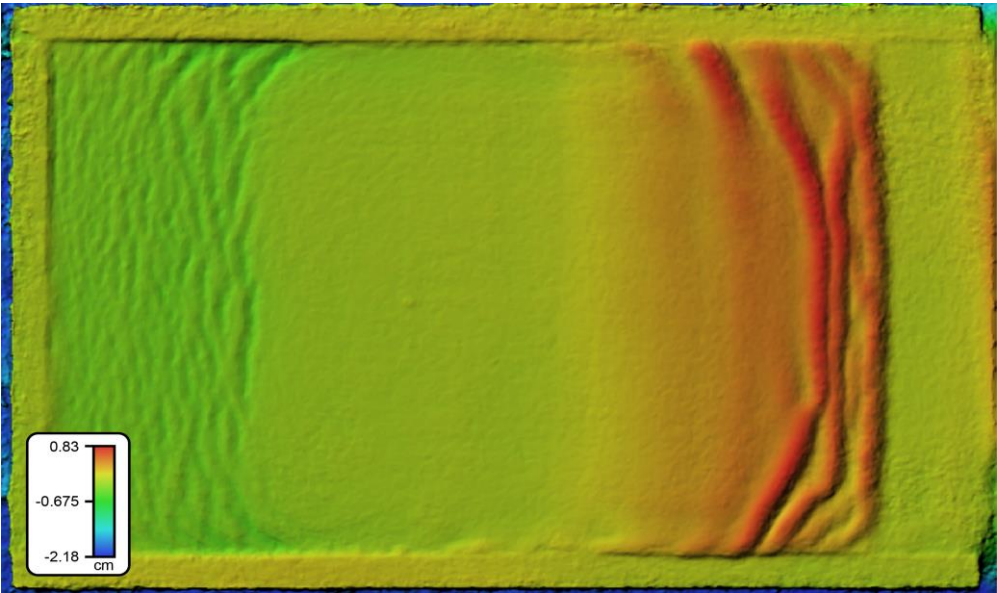
Figure 4: Example of normalized DEM file derived from SfM analysis (Model H). *Note that the actual data needed for topography analysis are included in these geotiff files.*

Table 3: Example of file with mesh and DEM parameters derived from photogrammetric reconstruction.

Model _time	n. of photos	n. of tie points	n. of dense cloud points	n. of Mesh faces	n. of markers	Mark. 1 coord. x/y (m)	Mark. 2 coord. x/y (m)	Mark. 3 coord. x/y (m)	Mark. 4 coord. x/y (m)	DEM resolution (mm/px)	Point cloud max. reprojection error
A_0h	17	14949	1841288	355756	4	0/0	0.68/0	0.68/0.40	0.68/0.40	0.471	0.462984 (18.268 pix)
A_48h	15	17620	3442296	277425	4	0/0	0.68/0	0.68/0.40	0.68/0.40	0.519	0.503826 (22.8004 pix)
...	...	...	...	...	...	...	...	...	...	...	...
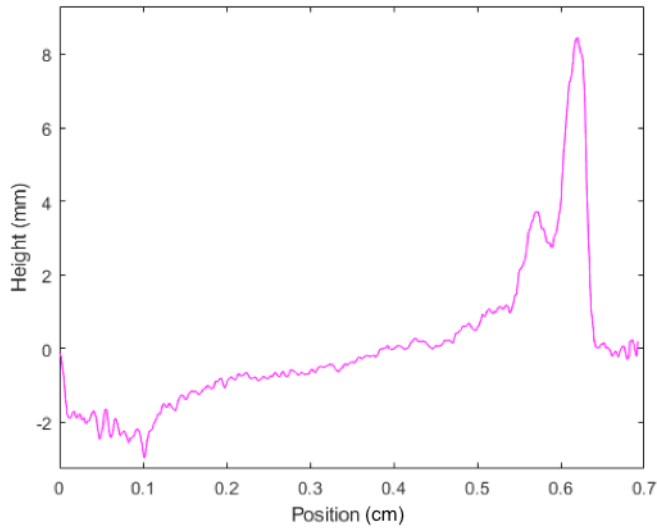
Figure 5: Example of a normalized DEM profile plot (Model F). Height along a down-slope profile at x=0 mm.

A Matlab-based script ("DEMprofilesPlot.m") is provided to automatically visualize height along the profile in a diagram (Figure 5). The input files are named "ID_DEM-y_x=0.txt" and contain two columns: Position and Height (Table 4).

Table 4: Example of DEM profile data file. The profile position and height values.

%position/mm	heigth/mm
0	-0.000141404
0.000703222	-0.000153792
...	...

4. File description

For each of the 35 experiments we provide PIV data:

    (i)   Movies of surface deformation ("ID_Dy_1h.avi")

    (ii)   Images of final surface displacement ("ID_Dy_48h.png")

    (iii)   Data of cumulative surface-displacement along a central profile ("ID_Dy-y-t_1h_x=0.prm")

    (iv)   Plot of cumulative surface-displacement along a central profile ("ID_Dy-y-t_1h_x=0.png")

    (v)   Matlab-script for plotting the Dy-profile data ("DyProfilesPlot.m")

    (vi)   Data of incremental surface-displacement along a central profile ("ID_Vy-y-t_8h_x=0.prm")

    (vii)   Plot of incremental surface-displacement along a central profile ("ID_Dy-y-t_8h_x=0.png")

    (viii)   Matlab-script for plotting the Vy-profile data ("VyProfilesPlot.m")

For 30 of the experiments we additionally provide SfM data:

    (ix)   Topography meshes at start (0h) and end (48h, or 49 h) of the experimental run ("ID_3D_time.pdf")

    (x)   Normalized digital elevation models with final model topography ("ID_DEM_time.tiff")

    (xi)   Normalized elevation data along a central profile ("ID_DEM-y_x=0.txt")

    (xii)   Matlab-script for plotting the DEM-profile data ("DEMplotProfiles.m")*

    (xiii)   Overview of mesh and DEM parameters for photogrammetric reconstruction ("3D_SfM_details.txt").

* For 20 models only

An overview of all files of the data set is given in the **List of Files.**

5. Acknowledgements

6. References

Adam, J., Urai, J. L., Wieneke, B., Oncken, O., Pfeiffer, K., Kukowski, N., Lohrmann, J., Hoth, S., van der Zee, W & Schmatz, J. (2005). Shear localisation and strain distribution during tectonic faulting – New insights from granular-flow experiments and high-resolution optical image correlation techniques. Journal of Structural Geology, 27(2), 283-301, https://doi.org/10.1016/j.jsg.2004.08.008

Donnadieu, F., Kelfoun, K., de Vries, B. V. W., Cecchi, E., & Merle, O. (2003). Digital photogrammetry as a tool in analogue modelling: applications to volcano instability. Journal of Volcanology and Geothermal Research, 123(1-2), 161-180. https://doi.org/10.1016/S0377-0273(03)00034-9

Westoby, M.J., Brasington, J., Glasser, N.F., Hambrey, M.J. & Reynolds, J.M. (2012): 'Structure-from-Motion' photogrammetry: A low-cost, effective tool for geoscience applications, Geomorphology, 179, 300-314, https://doi.org/10.1016/j.geomorph.2012.08.021

Zwaan, F., Rosenau, M., Maestrelli, D. (2021). How initial basin geometry influences gravity-driven salt tectonics: Insights from laboratory experiments. Marine and Petroleum Geology, 105195. https://doi.org/10.1016/j.marpetgeo.2021.105195